

CST-YOLO: A NOVEL METHOD FOR BLOOD CELL DETECTION BASED ON IMPROVED YOLOV7 AND CNN-SWIN TRANSFORMER

Ming Kang, Chee-Ming Ting*, Fung Fung Ting, Raphaël Phan

School of Information Technology, Monash University Malaysia

ABSTRACT

Blood cell detection is a typical small-scale object detection problem in computer vision. In this paper, we propose a CST-YOLO model for blood cell detection based on YOLOv7 architecture and enhance it with the CNN-Swin Transformer (CST), which is a new attempt at CNN-Transformer fusion. We also introduce three other useful modules: Weighted Efficient Layer Aggregation Networks (W-ELAN), Multiscale Channel Split (MCS), and Concatenate Convolutional Layers (CatConv) in our CST-YOLO to improve small-scale object detection precision. Experimental results show that the proposed CST-YOLO achieves 92.7, 95.6, and 91.1 mAP@0.5 respectively on three blood cell datasets, outperforming state-of-the-art object detectors, e.g., YOLOv5 and YOLOv7. Our code is available at <https://github.com/mkang315/CST-YOLO>.

Index Terms— Medical image processing, small object detection, deep learning, YOLO, CNN-Transformer fusion.

1. INTRODUCTION

Automated blood cell detection refers to recognizing different types of blood cells that include red blood cells (RBC), white blood cells (WBC), platelets, etc. in microscopic images. It is a crucial process for accurate blood cell count in pathology labs used for the diagnosis and treatment of different diseases. The main challenge in blood cell detection is that blood cells are small-scale objects for which traditional object detectors can only achieve sub-optimal performance. Faster Region-based Convolutional Neural Network (Faster R-CNN) [1, 2, 3] and YOLOv5 [3, 4] have achieved the best precision so far in automated detection of blood cells, where YOLOv5 performs better than Faster R-CNN [3].

YOLOv7 [5] is a cutting-edge object detector that surpasses YOLOv5 [6] and many other object detectors in speed and accuracy. The basic components of YOLOv7 networks that play a major role are ConvBNSiLU (or CBS), MPCConv, Extended Efficient Layer Aggregation Networks (E-ELAN), and Spatial Pyramid Pooling & Cross Stage Partial Network plus CBS (SPPCSPC). CBS is a Convolutional (Conv) layer followed by a Batch Normalization (BN) layer, and then finally a Sigmoid-weighted Linear Unit (SiLU) [7] as an activation function, which was firstly used by EfficientNet [8].

CBS replaces ConvBNLeakyReLU (or CBL) in YOLOv5 v4.0 and newer versions, and was also adopted by PP-YOLOv2 [9], YOLOX [10], PP-YOLOE [11] and YOLOv8 [12]. MPCConv connects two branches of a MaxPool + CBS layer and a CBS + CBS layer. E-ELAN controls the connection paths of different lengths so that the network has effective learning and convergence. Inspired by SPP [13] and CSPNet [14], SPPCSPC makes the head network suitable for multi-scale input and achieves a fusion of

different levels of features. Recently, [15] proposed Swin Transformer, a hierarchical transformer designed for computer vision tasks. It implements self-attention within local windows and establishes long-range cross-window dependency by shifted windowing scheme. A hybrid network of convolutional neural network (CNN) and Swin Transformer has been shown effective at both extracting contextual features and representing global long-range dependency features in detection and segmentation tasks [16, 17, 18].

In this paper, we propose an improved small object detection model called CST-YOLO, by leveraging both YOLOv7 and Swin Transformer [15] for blood cell detection. To our knowledge, CST-YOLO is the first object detector of Transformer with YOLOv7. The proposed CST-YOLO introduces several novel features in the YOLOv7 as follows:

- 1) We design a convolutional or CNN-Swin Transformer (CST) module based on Swin Transformer in the backbone and introduce it into the feature extraction module of YOLOv7, which can enhance the receptive field of the model and extract the target feature information better.
- 2) We develop an adaptive feature fusion module called Weighted ELAN (W-ELAN), which can dynamically fuse the feature map data with the effective feature map and restrain the invalid feature map.
- 3) We apply a Multiscale Channel Split (MCS) module to extract feature information from the input feature map with different receptive fields.
- 4) We build a Concatenation Convolutional Layers (CatConv) module to enhance the feature fusion capability and achieve better target detection by fusing more feature data.

Experimental evaluation on three blood cell datasets shows superior detection performance of CST-YOLO over YOLOv5 and YOLOv7.

2. METHODS

The proposed CST-YOLO model is shown in Fig. 1. It incorporates four new components in the YOLOv7, i.e., CST, W-ELAN, MCS, and CatConv.

2.1. CNN-Swin Transformer

To better capture global information in images, we design a CNN-Swin Transformer module (Fig. 2) and introduce it into YOLOv7 architecture. The CST firstly uses two parallel 1×1 convolutions to adjust the number of channels of the input feature map to obtain two outputs, one of which is used as input to the Swin Transformer, which captures the global feature information of the input feature map and then splices the two outputs. The CST module can extract features from the input feature map with different receptivity, which

* Corresponding author.

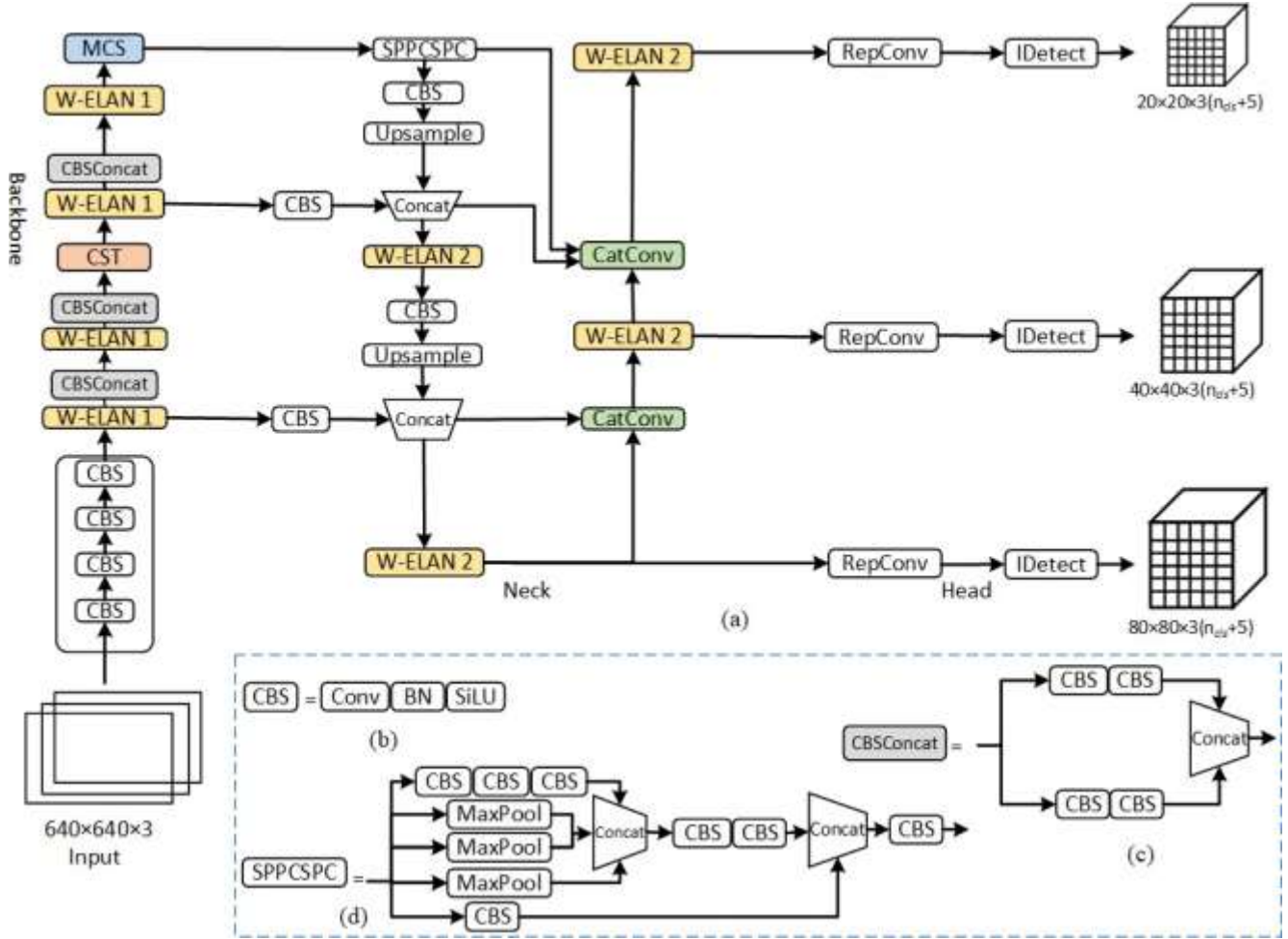


Fig. 1. (a) Overview of CST-YOLO. The architecture of CST-YOLO is based on YOLOv7 and incorporated new modules colored: CST, W-ELAN, MCS, and CatConv. The first CBS in the left of (c) CBSConcat replaces max pooling (MaxPool) in MPCConv of YOLOv7. (b) CBS, (d) SPPCSPC, RepConv and IDetect are existing modules in YOLOv7.

greatly improves the model’s ability to represent the input feature map, thus enhancing the model’s detection performance.

The Swin Transformer consists of two layers of self-attention mechanisms, using a normal window and shift window, respectively. At the former layer, the input feature map is first divided into windows (Fig. 3 (a)), then the self-attention mechanism is used for each window without any information interaction between the windows. This mechanism improves the detection speed but reduces the receptive field of the model, which is not conducive to feature extraction in the network. The shift window self-attention mechanism (Fig. 3 (b)) is subsequently introduced, where the window division of the normal window self-attention mechanism is first window-shifted, and the information in one window after the shift is equivalent to fusing multiple windows in the normal window self-attention mechanism.

For the blood cell image example in Fig. 3, the input of the window in the middle blue area in layer $i+1$ comes from the same area in layer i , while the blue area in layer $i+1$ contains the information of four windows in layer i . That is, each window in layer $i+1$ is equivalent to the information of four windows in layer i . This overcomes the problem that information can not be exchanged between different windows. By using both i -th and $i+1$ th layers in

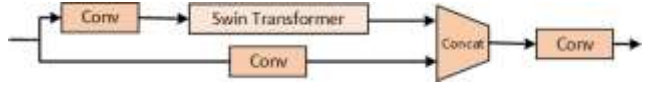


Fig. 2. The architecture of CNN-Swin Transformer module.

conjunction, it reduces the number of parameters as required in the traditional self-attention mechanism, and also alleviates the problem of the reduced receptive field of the normal window self-attention mechanism. By using the i -th and $i+1$ th layers in conjunction, not only can the problem of an excessive number of parameters in the traditional self-attention mechanism be solved, but also solved the problem that the receptive field of the normal window self-attention mechanism is reduced.

2.2. Weighted ELAN

Inspired by weighted feature fusion in EfficientDet [19], we develop a Weighted ELAN, a new variant different from E-ELAN [5, 20], to facilitate dynamic feature fusion. The architecture of W-ELAN is

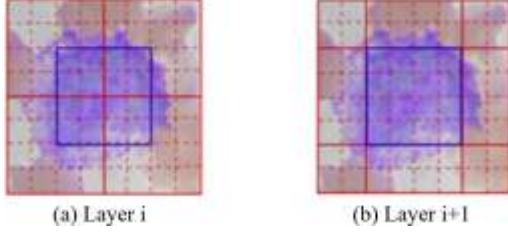


Fig. 3. The window and shift window of Swin Transformer.

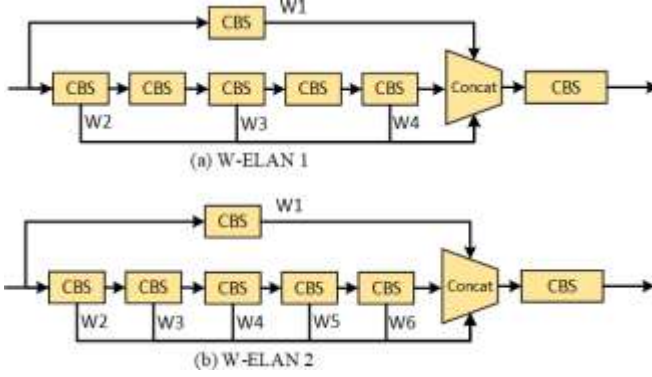


Fig. 4. The architectures of two variants of the Weighted ELAN module. (a) W-ELAN 1. (b) W-ELAN 2.

given in Fig. 4. A weight is applied to each feature map during the feature map splicing process, and it is a learnable parameter in the training process.

In order to prevent the weights w_i corresponding to different feature maps from varying greatly, the learned weights have to be normalized as follows

$$w_i = \frac{w'_i}{\sum_{j=0}^K w'_j + \xi} \quad (1)$$

where w_i is the normalized feature map weight, w'_i is the weight of the network output during training, and ξ is a fixed small value that prevents the denominator from being 0. During the training process, the network automatically assigns a larger weight to a feature if it makes a larger contribution to the final network's prediction, while a smaller weight is assigned to a feature with a smaller contribution to the final network's prediction. We noticed that this process is entirely determined by the training process without active jamming.

2.3. Multiscale Channel Split

Many studies have shown that significant differences exist in the extraction of target feature information in computer vision tasks with different settings of receptive field size in convolution. The smaller the receptive field is, the more localized image information can be observed in the network. Instead, the larger the receptive field is, the better the network is at understanding the global information of the input features. Drawing the idea of channel split in ShuffleNet V2 [21], we apply an MCS module (Fig. 5) to improve the model's ability to perceive target feature information at different scales.

The module passes the input feature maps through four different kernel average pooling layers to obtain feature maps of different sizes, then performs channel adjustment using $\times 1$ convolution to obtain four feature maps, where all channel numbers are 256. To concatenate the four feature maps, we first apply four up-sampling operations with different up-sampling coefficients to adjust the width and height of the four feature maps to a uniform size and then perform concatenation. Suppose the input feature map size is (B, C, W, H) , after the above operations, the output feature map is $(B, 1000, W, H)$. This feature map is then passed through the Average Pooling (AvgPool) where the average value of all the pixels in the batch is selected to obtain a feature map of size $(B, 1000, 1, 1)$, and after the Sigmoid activation function, the input feature values are normalized to between 0 and 1, which will be multiplied with the input feature map on the channel. This is equivalent to applying different attention to each channel of the input features, allowing the model to dynamically filter the channels with more feature information and suppress those with less.

To reduce the parameters of the MCS module, the feature map obtained after the above operations is divided into four along the channel direction, after which the four feature maps are summed, and the resulting feature maps are adjusted by using $\times 1$ convolution to the channel. A residual connection is also added to obtain the final output of the module.

2.4. Concatenate Convolutional Layers

To enhance the feature fusion capability of the model, we modify the MPCConv structure of the feature fusion part in Yolov7 by first replacing the max pooling (MaxPool) where the maximum pixel value of the batch is selected, hence producing CBSConcat in the backbone. Then, to extract more feature information using convolution, we multiply the relevant features from the downsampling part by 2 as the input to a Concatenate Convolutional Layers module (Fig. 6) in the neck. At the same time, to ensure the uni-size of the feature map, we adjust the size with a convolution whose step is 2 before feature fusion. In addition, we use RepConv + IDetect in YOLOv7 as the detection head. Essentially, RepConv is RepVGG [22] without identity connection and the latter is adopted in the reparameterizable backbone of YOLOv6 [23] and YOLOv6 v3.0 [24] at training.

3. EXPERIMENTAL RESULTS

3.1. Datasets

We evaluated the proposed CST-YOLO on three blood cell detection datasets, including Blood Cell Count and Detection (BCCD) [25], Complete Blood Count (CBC) [26, 27], and Blood Cell Detection (BCD) [28] datasets. These are small-scale object datasets with annotations of three classes of blood cells (WBC, RBC, and platelets). The three datasets differ in quantity, resolution, and division.

BCCD Dataset contains 364 images with 640×480 pixels. CBC dataset contains 360 blood smear images and each image is resized to 640×480 resolution. There are 364 images with 416×416 pixels resolution in the BCD dataset. The data partitioning of the three datasets into training, testing, and validation sets is given in Table 1. For CBC and BCD, we followed the original data partitioning as suggested in the sources of the datasets.

3.2. Implementation details

The CST-YOLO was trained with NVIDIA Telsa V100 and tested with NVIDIA RTX 2060. The hyperparameters used in the training

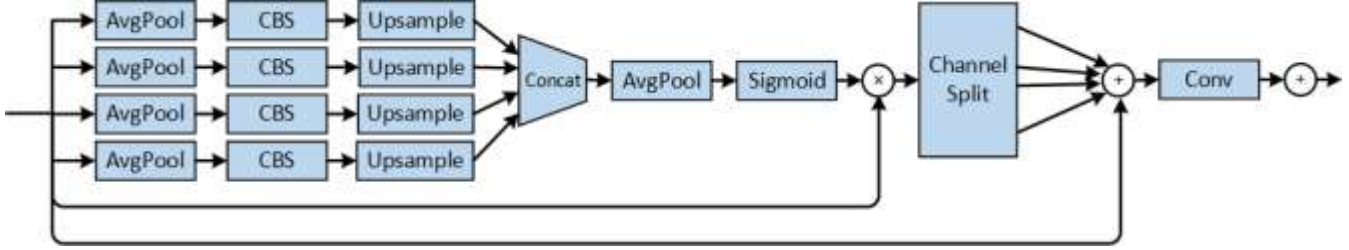


Fig. 5. The architecture of Multiscale Channel Split module.

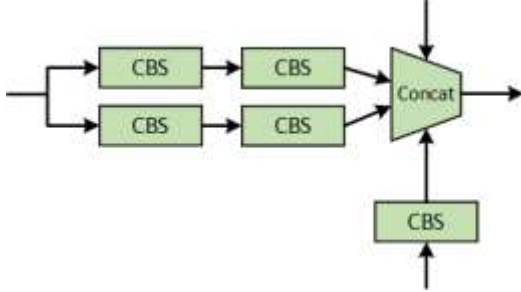


Fig. 6. The Concatenate Convolutional Layers module.

Table 1. Number of examples in BCCD, CBC, and BCD.

Dataset	Training	Validation	Testing	Total
BCCD	327	0	37	364
CBC	300	0	60	360
BCD	255	73	36	364

are a learning rate of 0.001 with a cosine annealing learning rate schedule and a weight decay rate of 0.0005. The training parameter batch size is set to 20 and the epoch is 150 in the learning phase.

3.3. Experimental Results

To evaluate object detection performance, we use average precision (AP) as metrics for each type of detected blood cell, and mean average precision (mAP) @0.5 (averages over all types) as the metric of the overall model. Table 2 shows the APs for different types of blood cells and mAP@0.5 using different detectors. We compare the proposed CST-YOLO with YOLOv5x v6.1 (no relevant updates on detection task in the newer versions of v6.2 and v7.0, only classification and segmentation checkpoints added in v6.2 and v7.0 respectively), YOLOv7. Results show that the CST-YOLO overall mAP@0.5 improved by 3.1%, 1.5%, and 3.7% respectively compared to the YOLOv7 results. AP values of the WBC, RBC, and platelets have all some improvement to YOLOv7. CST-YOLO even surpasses the extra large object detector YOLOv5x (86.7M parameters) which is twice larger than YOLOv7 (36.9M parameters) on the overall mAP.

3.4. Ablation Study

To validate which of the proposed modules plays a vital role in improving the accuracy of the dataset CBC, we investigate the effect on the performance of the proposed modules. We separately restore the original modules of YOLOv7 which are replaced by CST, W-ELAN,

Table 2. Performance comparison of YOLOv5x, YOLOv7 and CST-YOLO for blood cell detection. Results are APs for each blood cell type and mAP@0.5 for overall performance.

Dataset	Model	WBC	RBC	Platelets	Overall
BCCD	YOLOv5x	0.977	0.877	0.915	0.923
	YOLOv7	0.977	0.829	0.883	0.896
	CST-YOLO	0.984	0.869	0.928	0.927
CBC	YOLOv5x	0.995	0.930	0.942	0.955
	YOLOv7	0.995	0.917	0.912	0.941
	CST-YOLO	0.995	0.947	0.927	0.956
BCD	YOLOv5x	0.820	0.857	0.975	0.884
	YOLOv7	0.874	0.785	0.974	0.878
	CST-YOLO	0.899	0.857	0.978	0.911

Table 3. Abation study of the proposed CST-YOLO. Results are APs for each blood cell type and mAP@0.5 for overall performance.

Method	WBC	RBC	Platelets	Overall
w/o CST	0.999	0.944	0.923	0.955
w/o W-ELAN	0.995	0.954	0.910	0.953
w/o MCS	0.998	0.954	0.868	0.940
w/ MaxPool	0.999	0.920	0.938	0.952

MCS, and CatConv & CBSConcat (i.e., w/ MaxPool). In Table 3, it is seen that the overall mAP@0.5 of all methods that remove one of the proposed modules both decrease than CST-YOLO, so each proposed modules bring forth a positive effect on the improvement of CST-YOLO. the method without the MCS module has the biggest falls in the mAP@0.5, which demonstrate the importance of the MCS module is more crucial than others of our proposed modules in CST-YOLO. As platelets are the smallest and most indistinct objects in the images, another point of our analysis focuses on them. From decreasing values of APs on platelets, we judge the MCS module has a strong effect on the accuracy improvement of small blood cell detection, which is the key point influencing overall performance.

4. CONCLUSION

We develop a novel method CST-YOLO for small-scale object detection, by incorporating a CNN-Swin Transformer module in an improved YOLOv7-like architecture. Evaluated on blood cell detection on three benchmarking datasets, the proposed model provides substantially better detection precision than YOLOv5 and YOLOv7. This suggests that the incorporation of a CNN-Transformer fusion can potentially increase detection performance for small objects.

5. REFERENCES

- [1] S.-J. Lee, P.-Y. Chen, and J.-Y. M. Liao, "Complete blood cell detection and counting based on deep neural networks," *Appl. Sci.*, vol. 12, no. 16, Aug. 2022, p. 8140.
- [2] B. Hu, Y. Liu, P. Chu, M. Tong, and Q. Kong, "Small object detection via pixel level balancing with applications to blood cell detection," *Front. Physiol.*, vol. 13, Jun. 2022, p. 911297.
- [3] B. Liu, "Blood cell count and detection method based on yolo," in *Proc. Int. Conf. Electron. Sci. Autom. Remote. (ESAC)*, 2022, vol. 27, pp. 594–599.
- [4] J. Zhao, Y. Cheng, and X. Ma, "A real time intelligent detection and counting method of cells based on yolov5," in *Proc. IEEE Int. Conf. Electr. Eng. Big Data Algorithms (EEBDA)*, 2022, pp. 675–679.
- [5] C.-Y. Wang, A. Bochkovskiy, and H.-Y. M. Liao, "Yolov7: Trainable bag-of-freebies sets new state-of-the-art for real-time object detectors," arXiv:2207.02696v1 [cs.CV], Jul. 2022.
- [6] G. Jocher, "Yolov5 by ultralytics (version 7.0)," GitHub, 2022, <https://github.com/ultralytics/yolov5>.
- [7] S. Elfving, E. Uchibe, and K. Doya, "Sigmoid-weighted linear units for neural network function approximation in reinforcement learning," *Neural Netw.*, vol. 107, pp. 3–11, Nov. 2018.
- [8] M. Tan and Q. V. Le, "Efficientnet: Rethinking model scaling for convolutional neural networks," arXiv:1905.11946v5 [cs.LG], May 2020.
- [9] X. Huang *et al.*, "Pp-yolov2: A practical object detector," arXiv:2104.10419v1 [cs.CV], Apr. 2021.
- [10] Z. Ge, S. Liu, F. Wang, Z. Li, and J. Sun, "Yolox: Exceeding yolo series in 2021," arXiv preprint, arXiv:2107.08430v2 [cs.CV], Jul. 2021.
- [11] S. Xu *et al.*, "Pp-yoloe: An evolved version of yolo," arXiv:2203.16250v3 [cs.CV], Mar. 2022.
- [12] G. Jocher, A. Chaurasia, and J. Qiu, "Yolov8 by ultralytics," GitHub, 2023, <https://github.com/ultralytics/ultralytics>.
- [13] K. He, X. Zhang, S. Ren, and J. Sun, "Spatial pyramid pooling in deep convolutional networks for visual recognition," in *Proc. Eur. Conf. Comput. Vis. (ECCV)*, 2014, pp. 346–361.
- [14] C.-Y. Wang, H.-Y. M. Liao, Y.-H. Wu, P.-Y. Chen, J.-W. Hsieh, and I.-H. Yeh, "Cspnet: A new backbone that can enhance learning capability of cnn," in *Proc. IEEE/CVF Conf. Comput. Vis. Pattern Recog. Workshops (CVPRW)*, 2020, pp. 390–391.
- [15] Z. Liu *et al.*, "Swin transformer: Hierarchical vision transformer using shifted windows," in *Proc. IEEE/CVF Int. Conf. Comput. Vis. (ICCV)*, 2021, pp. 9992–10002.
- [16] Z. Liu, Y. Tan, Q. He, and Y. Xiao, "Swinnet: Swin transformer drives edge-aware rgb-d and rgb-t salient object detection," *IEEE Trans. Circuits Syst. Video Technol.*, vol. 32, no. 7, pp. 4486–4497, Jul. 2022.
- [17] Y. Guo, Y. Lan, and X. Chen, "Cst: Convolutional swin transformer for detecting the degree and types of plant diseases," *Comput. Electron. Agric.*, vol. 202, Nov. 2022, p. 107407.
- [18] H. Yang and D. Yang, "Cswin-pnet: A cnn-swin transformer combined pyramid network for breast lesion segmentation in ultrasound images," *Expert Syst. Appl.*, vol. 213, Part B, Mar. 2023, p. 119024.
- [19] M. Tan, R. Pang, and Q. V. Le, "Efficientdet: Scalable and efficient object detection," in *Proc. IEEE/CVF Conf. Comput. Vis. Pattern Recog. (CVPR)*, 2020, pp. 10781–10790.
- [20] C.-Y. Wang, H.-Y. M. Liao, and I.-H. Yeh, "Designing network design strategies through gradient path analysis," arXiv:2211.04800v1 [cs.CV], Nov. 2022.
- [21] N. Ma, X. Zhang, H.-T. Zheng, and J. Sun, "Shufflenet v2: Practical guidelines for efficient cnn architecture design," in *Proc. Eur. Conf. Comput. Vis. (ECCV)*, 2018, pp. 116–131.
- [22] X. Ding, X. Zhang, N. Ma, J. Han, G. Ding, and J. Sun, "Repvgg: Making vgg-style convnets great again," in *Proc. IEEE/CVF Conf. Comput. Vis. Pattern Recog. (CVPR)*, 2021, pp. 13733–13742.
- [23] C. Li *et al.*, "Yolov6: A single-stage object detection framework for industrial applications," arXiv:2209.02976v1 [cs.CV], Sep. 2022.
- [24] C. Li *et al.*, "Yolov6 v3.0: A full-scale reloading," arXiv:2301.05586v1 [cs.CV], Jan. 2023.
- [25] S. Cheng, "Bccd (blood cell count and detection) dataset," GitHub, 2019, <https://github.com/Shenggan/BCCD.Dataset>.
- [26] M. M. Alam and M. T. Islam, "Machine learning approach of automatic identification and counting of blood cells," *Healthc. Technol. Lett.*, vol. 6, no. 4, pp. 103–108, Aug. 2019.
- [27] M. M. Alam, "Complete blood count (cbc) dataset," GitHub, 2021, <https://github.com/MahmudulAlam/Complete-Blood-Cell-Count-Dataset>.
- [28] A. Dongre, "Blood cell detection dataset," Kaggle, 2021, <https://www.kaggle.com/datasets/adhoppin/blood-cell-detection-dataset>.